






RESEARCH ARTICLE | FEBRUARY 16 2024

Electrolyte gated graphene terahertz amplitude modulators

Syed Muhammad Abouzar Sarfraz ; Alessandra Di Gaspare ; Miriam Serena Vitiello ; Gaetano Scamarcio  



Appl. Phys. Lett. 124, 071114 (2024)

<https://doi.org/10.1063/5.0176096>



03 July 2024 07:37:52



Applied Physics Letters

Special Topic:

Quantum Networks

Guest Editors: David Awschalom, Ronald Hanson, Stephanie Simmons

[Submit Today!](#)

Electrolyte gated graphene terahertz amplitude modulators

Cite as: Appl. Phys. Lett. **124**, 071114 (2024); doi: [10.1063/5.0176096](https://doi.org/10.1063/5.0176096)

Submitted: 30 November 2023 · Accepted: 23 January 2024 ·

Published Online: 16 February 2024




View Online



Export Citation



CrossMark

Syed Muhammad Abouzar Sarfraz,^{1,2}  Alessandra Di Gaspare,³  Miriam Serena Vitiello,³ 
and Gaetano Scamarcio^{1,2,a)} 

AFFILIATIONS

¹Dipartimento Interateneo di Fisica, Università degli studi di Bari Aldo Moro, I-70125 Bari, Italy

²CNR-Istituto di Fotonica e Nanotecnologie, Bari I-70125, Italy

³NEST, CNR-NANO and Scuola Normale Superiore Pisa, Pisa I-56127, Italy

^{a)} Author to whom correspondence should be addressed: gaetano.scamarcio@uniba.it

ABSTRACT

Active manipulation of the amplitude of terahertz (THz) frequency waves, through electrical tuning, is key for next-generation THz imaging and essential for unlocking strategic applications, from wireless communication to quantum technologies. Here, we demonstrate high-performance THz amplitude modulators based on an electrolyte-gated single-layer graphene. Broadband modulation in the 1.5–6 THz range is achieved by optimizing the electric field coupling by carefully controlling the spacer thickness in a quarter-wavelength cavity structure, with a maximum modulation depth of 40% at around 2 THz. Raman characterization confirms a Fermi-level tuning of 0.39 eV via electrolyte gating of graphene. A test 2×2 modulator array with independent control of sub-millimeter regions is then developed and tested, with no crosstalk between pixels. The reported results highlight the potential of electrolyte-gated graphene for efficient THz modulation. The single-chip design offers compactness and ease of integration with other electronic components, making it a promising platform for THz spatial light modulators and adaptive optical components.

© 2024 Author(s). All article content, except where otherwise noted, is licensed under a Creative Commons Attribution (CC BY) license (<http://creativecommons.org/licenses/by/4.0/>). <https://doi.org/10.1063/5.0176096>

There is an increasing interest in optoelectronic devices operating in the 0.1–10 THz frequency range of the electromagnetic spectrum for applications in spectroscopy,^{1,2} imaging,³ wireless communications,^{4,5} and quantum technologies.⁶ Unlocking the full potential of these technologies requires efficient amplitude, frequency, and phase modulation of terahertz (THz) waves. In quantum technologies, such as quantum key distribution (QKD) systems, the modulation of single terahertz photons' amplitude, phase, and polarization state introduces interesting capabilities for quantum communication and computing.^{7,8} Additionally, THz modulators provide opportunities to study fundamental phenomena in THz quantum cascade lasers.^{6,9}

Significant improvements in controlling various properties of THz electromagnetic waves, such as amplitude,^{10,11} phase,^{12,13} frequency,^{14,15} and polarization^{16,17} in the 0.1–10 THz range with an amplitude modulation (AM) depth reaching 100% (Ref. 18) and high-speed (14 GHz) optical signal switching¹⁹ have been reported. However, dynamically manipulating electromagnetic wave propagation in the THz band remains challenging, necessitating ultrafast electronics and active materials. Over the past two decades, extensive efforts have targeted developing active THz devices with controllable

amplitude and phase.^{20–24} Early approaches focused on cooled semiconductor quantum wells with intersubband absorption in the THz range.²⁵ By depleting electrons, absorption can be reduced and reflection increased. Metamaterials have also been explored to amplify these interactions.

Two-dimensional (2D) materials, especially graphene, provide original avenues for manipulating light–matter interactions across the THz. In the THz, the optical conductivity σ of single-layer graphene (SLG) is dominated by intraband transitions. Following the Drude model, $\sigma = iD/\pi(\omega + i\Gamma)$, where $D = (v_F e^2 / \hbar) \sqrt{\pi |n|}$, v_F is the Fermi velocity, and n is carrier density.²⁶ Through electrostatic gating, the graphene's carrier density, the Fermi level and the complex optical conductivity can be tuned, enabling amplitude, phase, or polarization modulation to THz frequencies.^{27–29} However, challenges with fabrication, doping uniformity, and contact resistance must still be overcome to fully exploit graphene's potential for high-performance THz modulators.

Electrolyte gating (EG) emerges as a powerful technique for tuning graphene's optoelectronic properties. Unlike solid dielectrics, ionic liquids can create large electric double layers (EDLs) at the graphene

interface, shifting the Fermi level by over 1 eV at low biases (<3 V).^{30,31} The self-assembled nanoscale EDL acts as a nanocapacitor, spontaneously generating intense 10^9 V/m electric fields over tiny distances without electrical breakdown. The EDL's self-formation in large area provides electrolyte gating with high charge storage capacity without complex manufacturing. By combining such strong electrostatic doping with graphene's inherent tunable conductivity and high mobility, breakthroughs in THz modulators, switches, and metamaterials are envisioned. Further improvements in speed³² stability³³ and integration³⁴ of electrolyte-gated graphene could enable fast, low-power, and CMOS-compatible THz modulation.

To realize an amplitude modulator structure, the gated graphene layer is conveniently placed at a distance of one-quarter wavelength ($\lambda/4$) from a reflective metallic surface, where the amplitude of the created stationary wave is maximum.^{35,36} Remarkably, the reflectivity of the heterostructure can be controlled by varying the gate voltage.

Here, we report on high-performance THz amplitude modulators using electrolyte-gated SLG in reflection geometry. By optimizing the spacer thickness to maximize electric field coupling at the graphene/electrolyte interface and utilizing resonance effects, we achieve broadband (1.5–6 THz) modulation with 40% modulation depth for applied voltages in the range $[-0.5, +0.5$ V]. Raman spectroscopy confirms a large shift by 13.6 cm^{-1} of the G peak, corresponding to a Fermi level shift of 0.39 eV. We also present a 2×2 spatial light modulator array with independent control of sub-millimeter scale regions and no crosstalk between pixels.

The devised THz modulators employ a reflective architecture consisting of a graphene/electrolyte/metal stack [Figs. 1(a) and 1(b)]. The electrolyte is DEME TFSI (N,N-diethyl N-methyl-N-(2-methoxyethyl ammonium bis-trifluoromethanesulfonyl imide—99.9%). A commercially available polycarbonate spacer with actual thicknesses (15.5, 16.5, and 47 μm) defines a 3×3 mm^2 cavity filled with the ionic liquid electrolyte. This active region is sandwiched between SLG and a glass substrate coated with 5/200 nm of the Ti/Au thin film mirror deposited by e-beam evaporation. Commercial SLG films deposited on quartz substrates (Graphenea, Inc.) are employed. Meticulous stacking of the quartz/SLG on the top of the spacer/electrolyte/metal structure completes the modulator structure.

The devices are then characterized by measuring the electrical resistance, the *in situ* and operando Raman spectra, and the THz power reflectance, as a function of the applied gate voltage (V_G). The resistance–voltage characteristics of Fig. 1(c) exhibit well-defined peaks at 0.0, 0.2, and 0.0 V for devices with active layer thicknesses of 15.5,

16.5, and 47 μm , respectively. The peaks correspond to the charge neutrality point (CNP) of SLG.³⁷

We employed Raman spectroscopy to investigate the gate-tunable response of the electrolyte-gated graphene modulators. Raman measurements are performed in the range V_G $[-0.5, +0.5$ V] with 0.05 V steps. The applied voltage creates electric double layers (EDLs) at the SLG/electrolyte and at the Au/electrolyte reflector that modulate the SLG carrier density and the Fermi energy. A low voltage range is used to avoid electrochemical processes. Raman spectra are acquired at each V_G . The G band corresponds to the E_{2g} phonon at the Brillouin-zone center (Γ point), which is a second-order vibration caused by the scattering of phonons at the zone boundary.^{38,39} The 2D band is the second order of the D band (defect band).⁴⁰

Figures 2(a) and 2(b) show the Raman spectra recorded on a representative device having a spacer thickness $S = 15.5$ μm , in the regions of G (left) and 2D (right) peaks. A Lorentzian fitting of the voltage-dependent G and 2D peaks [Figs. 2(a) and 2(b)] allows the extraction of key parameters: G and 2D central frequencies, G peak full width at half maximum (FWHM), and 2D/G intensity ratios, which are plotted in Figs. 2(c)–2(f). See the supplementary material for details.

The Fermi energy depends on the energy of the G peak as^{31,40}

$$|E_F| = \frac{2\pi\hbar\omega_G M v_F^2}{A_{uc} D^2} (\hbar\omega_G - \hbar\omega_G^0), \quad (1)$$

where $\hbar\omega_G$ is the G band energy; $\hbar\omega_G^0$ is the G band energy at CNP; D is the electron–phonon coupling strength, 12.6 $\text{eV}/\text{\AA}$; A_{uc} is the area of the graphene honeycomb unit cell, 0.051 nm^2 ; M is the carbon atom mass, 1.993×10^{-26} kg; and v_F is the Fermi velocity, 1.2×10^6 m/s.

From the minimum $\hbar\omega_G$ value in the explored voltage range, corresponding to 1584.4 cm^{-1} , we can estimate a CNP of -0.05 V, which matches well the value found through resistance–voltage measurements shown in Fig. 1(c). From the change by 13.6 cm^{-1} of $\hbar\omega_G$, a maximum Fermi energy shift of 0.39 eV, is extracted. Also, the G peak FWHM decreases by a factor of 2.2 [Fig. 2(e)]. The 2D/G intensity ratio reaches a maximum at the CNP and decreases as the SLG is biased, starting to saturate at higher bias voltages. This comprehensive Raman description reveals the voltage-controlled tunability of graphene's vibrational properties, which are directly related to the change in Fermi energy and free carrier concentration and hence anticipate the corresponding THz reflectivity modulation. Gate tunable response of graphene-based electrolyte gated THz modulators for spacer thickness 16.5 and 47 μm are described in the supplementary material Figs. S3 and S4, respectively.

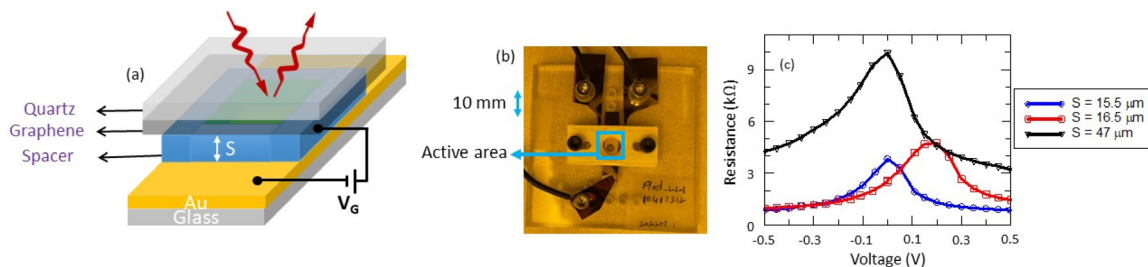


FIG. 1. (a) Graphene modulator scheme consisting of a 3×3 mm^2 electrolyte-filled cavity sandwiched between single-layer graphene (SLG) and a gold back reflector. The modulation occurs in the reflection mode by applying a bias voltage between the SLG and the back reflector surface Au. (b) Optical image of the terahertz modulator. (c) Measured device resistance as a function of the biased voltage. The peaks in the individual curves correspond to the CNP of SLG.

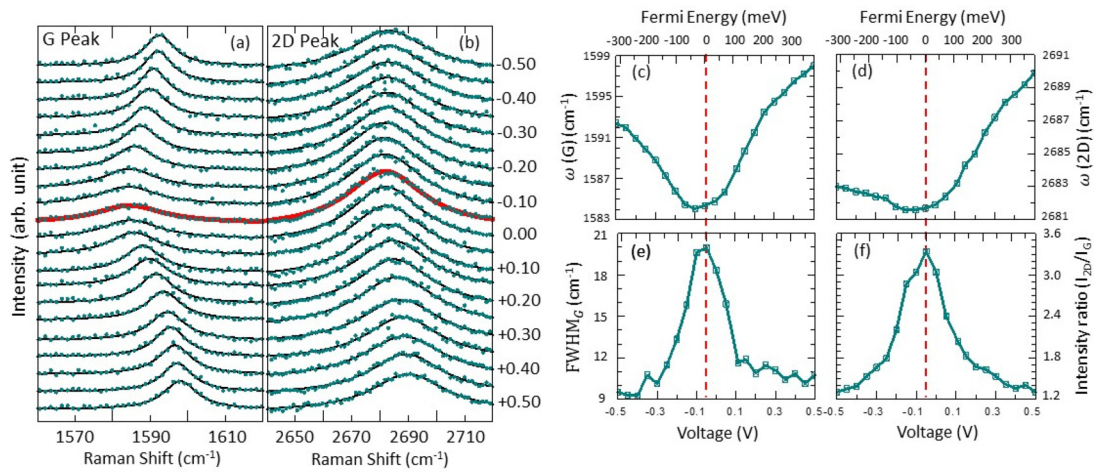


FIG. 2. Raman spectra of the THz modulator with $15.5 \mu\text{m}$ thick spacer, as a function of V_G . Bands due to G and 2D phonons (a) and (b) are fitted with Lorentzian functions (black lines). Applied voltage dependence of G peak (c), 2D peak (d), G peak full width at half maximum (FWHM) (e), and 2D/G peak intensity ratio (f). The standard error was found to be $\sim 1\%$, and the error bars are smaller than the marker size and are not shown.

Fourier transform infrared spectroscopy is employed to measure the THz reflectivity modulation as a function of V_G , normalized to a gold mirror reference [Fig. 3(a)] (see the supplementary material Fig. S5). The modulation efficiency is quantified by the modulation depth [Fig. 3(b)], calculated as $\eta = 100 \times \left(\frac{R(V_{\text{CNP}}) - R(V_G)}{R(V_{\text{CNP}})} \right)$. $R(V_G)$ is the reflectivity at gate voltage V_G and $R(V_{\text{CNP}})$ is the maximum reflectivity at the charge neutrality point.²⁶ A maximum modulation depth $\eta = 40\%$ is attained, demonstrating efficient tuning of THz reflectivity in these graphene modulators. A good agreement with the calculated frequency dependence of the electric field intensity [Fig. 3(c)] is found. The results for spacer thicknesses 16.5 and $47 \mu\text{m}$ show a similar behavior and are shown in the supplementary material (Figs. S6 and S7, respectively). These are compared with the results found for spacer thickness of $15.5 \mu\text{m}$ and summarized in Table I.

As a proof of principle toward the fabrication of a spatial light modulator, four independent ($13 \times 3 \text{ mm}^2$) pixels separated by 0.3 mm gaps are defined on a glass substrate by e-beam evaporation of Ti/Au ($5/200 \text{ nm}$). Four $47 \mu\text{m}$ -thick optical tissue spacers soaked in ionic liquid create $5 \times 3 \text{ mm}^2$ active regions sandwiched between the continuous SLG and the individual pixel metal layers. This forms a 2×2 submillimeter pixel array operated in reflection mode, with the

common SLG top contact and distinct spacer/reflector for each individually addressable $200 \times 200 \mu\text{m}^2$ pixel.

The spatial light modulator array comprises four independently addressable pixels. Graphene charge density modulation is monitored through *in situ* micro-probe Raman spectroscopy. Electrolyte gating allows Fermi level tuning up to 0.5 eV with remarkably low [-0.5 , $+0.5 \text{ V}$] voltages and without crosstalk. Figure 4(b) shows Raman spectra for pixel 3. Varying the gate bias from -0.5 to $+0.5 \text{ V}$, the G band of pixel 3 is tuned, demonstrating localized graphene gating. Interestingly, the G band of pixel 3 shows no tuning when pixel 1 is biased, indicating that the pixels are well isolated. This demonstrates the capability to fabricate modulator arrays without crosstalk and independent pixel operation using electrolyte gating, which has not been reported previously. Exploiting this approach could enable efficient THz spatial light modulators comparable to state-of-the-art devices^{41–44} and provide a path toward high-performance terahertz spatial light modulators.

In conclusion, we have demonstrated amplitude modulators at THz frequencies using electrolyte-gated single-layer graphene positioned at a distance of one-quarter wavelength ($\lambda/4$) from the metallic reflecting surface. By precisely controlling the electric field coupling between the graphene/electrolyte interfaces, as well as exploiting resonant effects via different spacer thicknesses, we achieved modulation

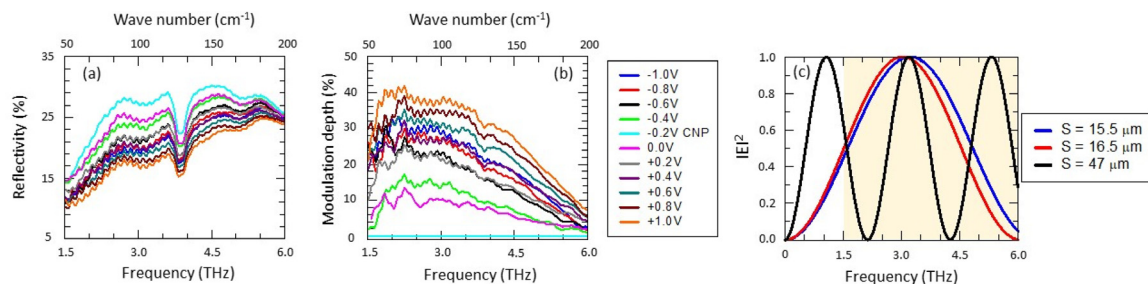


FIG. 3. THz reflectivity spectrum (a) and modulation depth (b) as a function of the applied voltage V_G . (c) Electric field intensity calculated as a function of the radiation frequency for spacer thickness $S = 15.5$, 16.5 , and $47 \mu\text{m}$.

TABLE I. Analysis of the single pixel modulator for different spacer thicknesses.

Modulator	Spacer thickness (μm)	CNP extracted by electrical measurement (V)	CNP extracted from FTIR (V)	CNP extracted from Raman (V)	Modulation depth (%)	Broadband (THz)
1	15.5	0	-0.2	-0.05	40	1.5–6.0
2	16.5	0.2	-0.1	0.00	36	1.5–6.0
3	47	0	-0.2	-0.15	22	1.5–6.0

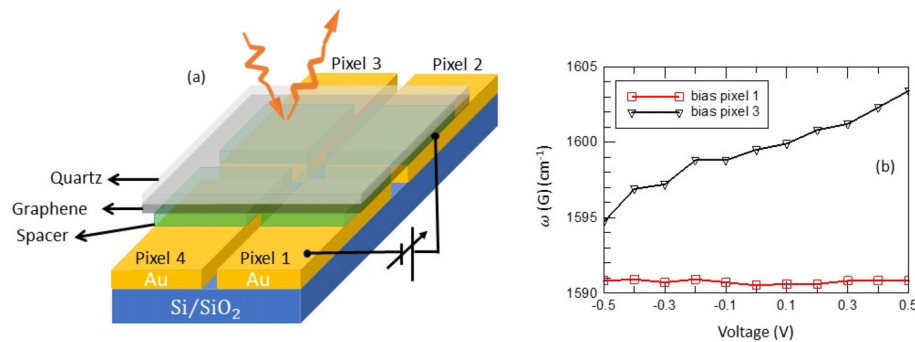


FIG. 4. (a) Schematic of the multi-pixel modulator array. (b) Raman spectra demonstrate independent pixel addressing. Pixel 3 exhibits gate-tuning of ω_G band when biased, while no tuning of ω_G band is seen when pixel 1 is biased that exhibits independent operation.

depths exceeding 40%. By varying the spacer thicknesses, we show that the 15.5 μm spacer showed the broadest tuning range of 1.5–6 THz, owing to optimal resonance conditions. Raman analysis confirmed that a mere bias voltage range of ± 0.5 V resulted in an impressive 13.6 cm^{-1} modulation of the G peak frequency, and a Fermi-level tuning of 0.39 eV, thereby validating the underlying tuning mechanisms. Finally, we fabricated a 2×2 spatial light modulator array, where independent addressing and control over sub-millimeter scale regions of graphene were achieved without any crosstalk between pixels. These results pave the way for the development of high-performance THz modulators and open up possibilities for their integration for different applications, such as spectroscopy and imaging. The monolithic integration of electrolyte-gated graphene structures with existing CMOS terahertz technology will enable the realization of highly compact terahertz systems on a single chip.

See the supplementary material for details on the fabrication of single and multi-pixel THz modulators, the calculation of the reflectivity as a function of the voltage-induced Fermi energy shift, additional Raman results on modulators with spacer thickness of 16.5 and 47 μm , and the data processing of the reflectivity modulation and efficiency.

This article was supported by the European Union under the Italian National Recovery and Resilience Plan (NRRP) of NextGenerationEU, partnership on “Telecommunications of the Future” (PE00000001 - program “RESTART”, Project MIND-DREAMS and T-NEXT).

AUTHOR DECLARATIONS

Conflict of Interest

The authors have no conflicts to disclose.

Author Contributions

Syed Muhammad Abouzar Sarfraz: Conceptualization (equal); Data curation (equal); Formal analysis (equal); Investigation (equal); Writing – original draft (equal). **Alessandra Di Gaspare:** Formal analysis (equal); Investigation (equal). **Miriam Serena Vitiello:** Project administration (equal); Writing – review & editing (equal). **Gaetano Scamarcio:** Conceptualization (equal); Supervision (equal); Writing – review & editing (equal).

DATA AVAILABILITY

The data that support the findings of this study are available within the article and its supplementary material.

REFERENCES

- P. U. Jepsen, D. G. Cooke, and M. Koch, “Terahertz spectroscopy and imaging—Modern techniques and applications,” *Laser Photonics Rev.* **5**, 124–166 (2011).
- Y. Ozaki, “Infrared spectroscopy—Mid-infrared, near-infrared, and far-infrared/terahertz spectroscopy,” *Anal. Sci.* **37**, 1193–1212 (2021).
- D. M. Mittleman, “Twenty years of terahertz imaging [Invited],” *Opt. Express* **26**, 9417–9431 (2018).
- I. F. Akyildiz, J. M. Jornet, and C. Han, “Terahertz band: Next Frontier for wireless communications,” *Phys. Commun.* **12**, 16–32 (2014).
- Z. Chen, B. Ning, C. Han, Z. Tian, and S. Li, “Intelligent reflecting surface assisted terahertz communications toward 6G,” *IEEE Wireless Commun.* **28**, 110–117 (2021).
- M. S. Vitiello and P. De Natale, “Terahertz quantum cascade lasers as enabling quantum technology,” *Adv. Quantum Technol.* **5**, 2100082 (2021).
- A. Sigov, L. Ratkin, L. A. Ivanov, and L. Da Xu, “Emerging enabling technologies for industry 4.0 and beyond,” *Inf. Syst. Front.* **1**, 1–11 (2022).
- Z. Wang, R. Malaney, and J. Green, “Inter-satellite quantum key distribution at terahertz frequencies,” in *IEEE International Conference on Communications* (IEEE, 2019).

- ⁹A. Di Gaspare, E. A. A. Pogna, E. Riccardi, S. M. A. Sarfraz, G. Scamarcio, and M. S. Vitiello, "All in one-chip, electrolyte-gated graphene amplitude modulator, saturable absorber mirror and metrological frequency-tuner in the 2–5 THz range," *Adv. Opt. Mater.* **10**, 2200819 (2022).
- ¹⁰P. Gopalan, B. Sensale-Rodriguez, P. Gopalan, and B. Sensale-Rodriguez, "2D materials for terahertz modulation," *Adv. Opt. Mater.* **8**, 1900550 (2020).
- ¹¹E. Heidari, H. Dalir, F. M. Koushyar, B. M. Nouri, C. Patil, M. Miscuglio, D. Akinwande, and V. J. Sorger, "Integrated ultra-high-performance graphene optical modulator," *Nanophotonics* **11**, 4011–4016 (2022).
- ¹²H. T. Chen, W. J. Padilla, M. J. Cich, A. K. Azad, R. D. Averitt, and A. J. Taylor, "A metamaterial solid-state terahertz phase modulator," *Nat. Photonics* **3**, 148–151 (2009).
- ¹³H. Zeng, S. Gong, L. Wang, T. Zhou, Y. Zhang, F. Lan, X. Cong, L. Wang, T. Song, Y. Zhao, Z. Yang, and D. M. Mittleman, "A review of terahertz phase modulation from free space to guided wave integrated devices," *Nanophotonics* **11**, 415–437 (2022).
- ¹⁴N. Mou, B. Tang, J. Li, H. Dong, and L. Zhang, "Switchable ultra-broadband terahertz wave absorption with VO₂-based metasurface," *Sci. Rep.* **12**, 2501 (2022).
- ¹⁵Y. Hu, M. Tong, X. Cheng, J. Zhang, H. Hao, J. You, X. Zheng, and T. Jiang, "Bi₂Se₃-functionalized metasurfaces for ultrafast all-optical switching and efficient modulation of terahertz waves," *ACS Photonics* **8**, 771–780 (2021).
- ¹⁶C. J. Gao, Y. Z. Sun, and H. F. Zhang, "Tunable dual-band linear-to-circular polarization conversion based on the electromagnetically induced transparency utilizing the graphene metamaterial," *Physica E* **141**, 115225 (2022).
- ¹⁷Q. Sun, X. Chen, X. Liu, R. I. Stantchev, and E. Pickwell-MacPherson, "Exploiting total internal reflection geometry for terahertz devices and enhanced sample characterization," *Adv. Opt. Mater.* **8**, 1900535 (2020).
- ¹⁸G. Liang, X. Hu, X. Yu, Y. Shen, L. H. Li, A. G. Davies, E. H. Linfield, H. K. Liang, Y. Zhang, S. F. Yu, and Q. J. Wang, "Integrated terahertz graphene modulator with 100% modulation depth," *ACS Photonics* **2**, 1559–1566 (2015).
- ¹⁹P. K. Singh and S. Sonkusale, "High speed terahertz modulator on the chip based on tunable terahertz slot waveguide," *Sci. Rep.* **7**, 40933 (2017).
- ²⁰S. H. Lee, M. Choi, T. T. Kim, S. Lee, M. Liu, X. Yin, H. K. Choi, S. S. Lee, C. G. Choi, S. Y. Choi, X. Zhang, and B. Min, "Switching terahertz waves with gate-controlled active graphene metamaterials," *Nat. Mater.* **11**, 936–941 (2012).
- ²¹H.-T. Chen, W. J. Padilla, J. M. O. Zide, A. C. Gossard, A. J. Taylor, and R. D. Averitt, "Active terahertz metamaterial devices," *Nature* **444**, 597–600 (2006).
- ²²B. Sensale-Rodriguez, R. Yan, M. M. Kelly, T. Fang, K. Tahy, W. S. Hwang, D. Jena, L. Liu, and H. G. Xing, "Broadband graphene terahertz modulators enabled by intraband transitions," *Nat. Commun.* **3**, 780 (2012).
- ²³I. C. Benea-Chelmus, S. Mason, M. L. Meretska, D. L. Elder, D. Kazakov, A. Shams-Ansari, L. R. Dalton, and F. Capasso, "Gigahertz free-space electro-optic modulators based on Mie resonances," *Nat. Commun.* **13**, 3170 (2022).
- ²⁴N. Kakenov, M. S. Ergoktas, O. Balci, and C. Kocabas, "Graphene based terahertz phase modulators," *2D Mater.* **5**, 035018 (2018).
- ²⁵S. I. Borenstain and J. Katz, "Evaluation of the feasibility of a far-infrared laser based on intersubband transitions in GaAs quantum wells," *Appl. Phys. Lett.* **55**, 654–656 (1989).
- ²⁶A. Di Gaspare, E. Arianna Aurelia Pogna, L. Salemi, O. Balci, A. Ronieri Cadore, S. Maruti Shinde, L. Li, C. di Franco, A. Giles Davies, E. Harold Linfield, A. Carlo Ferrari, G. Scamarcio, M. Serena Vitiello, A. Di Gaspare, E. A. A. Pogna, L. Salemi, M. S. Vitiello, O. Balci, A. R. Cadore, S. M. Shinde, A. C. Ferrari, L. Li, A. G. Davies, and E. H. Linfield, "Tunable, grating-gated, graphene-on-polyimide terahertz modulators," *Adv. Funct. Mater.* **31**, 2008039 (2021).
- ²⁷R. Ulbricht, E. Hendry, J. Shan, T. F. Heinz, and M. Bonn, "Carrier dynamics in semiconductors studied with time-resolved terahertz spectroscopy," *Rev. Mod. Phys.* **83**, 543–586 (2011).
- ²⁸E. A. A. Pogna, A. Tomadin, O. Balci, G. Soavi, I. Paradisanos, M. Guizzardi, P. Pedrinazzi, S. Mignuzzi, K.-J. Tielrooij, M. Polini, A. C. Ferrari, and G. Cerullo, "Electrically tunable nonequilibrium optical response of graphene," *ACS Nano* **16**, 3613–3624 (2022).
- ²⁹A. Das, S. Pisana, B. Chakraborty, S. Piscanec, S. K. Saha, U. V. Waghmare, K. S. Novoselov, H. R. Krishnamurthy, A. K. Geim, A. C. Ferrari, and A. K. Sood, "Monitoring dopants by Raman scattering in an electrochemically top-gated graphene transistor," *Nat. Nanotechnol.* **3**, 210–215 (2008).
- ³⁰O. Balci, E. O. Polat, N. Kakenov, and C. Kocabas, "Graphene-enabled electrically switchable radar-absorbing surfaces," *Nat. Commun.* **6**, 6628 (2015).
- ³¹M. Bruna, A. K. Ott, M. Ijäs, D. Yoon, U. Sassi, and A. C. Ferrari, "Doping dependence of the Raman spectrum of defected graphene," *ACS Nano* **8**, 7432–7441 (2014).
- ³²A. M. Zaman, Y. Lu, X. Romain, N. W. Almond, O. J. Burton, J. Alexander-Webber, S. Hofmann, T. Mitchell, J. D. P. Griffiths, H. E. Beere, D. A. Ritchie, and R. Degl'innocenti, "Terahertz metamaterial optoelectronic modulators with GHz reconfiguration speed," *IEEE Trans. Terahertz Sci. Technol.* **12**, 520–526 (2022).
- ³³Z. Ren, J. Xu, J. Liu, B. Li, C. Zhou, and Z. Sheng, "Active and smart terahertz electro-optic modulator based on VO₂ structure," *ACS Appl. Mater. Interfaces* **14**, 26923–26930 (2022).
- ³⁴S. Venkatesh, X. Lu, H. Saeidi, and K. Sengupta, "A high-speed programmable and scalable terahertz holographic metasurface based on tiled CMOS chips," *Nat. Electron.* **3**, 785–793 (2020).
- ³⁵M. S. Jang, V. W. Brar, M. C. Sherrott, J. J. Lopez, L. Kim, S. Kim, M. Choi, and H. A. Atwater, "Tunable large resonant absorption in a midinfrared graphene Salisbury screen," *Phys. Rev. B* **90**, 165409 (2014).
- ³⁶A. Di Gaspare, E. A. A. Pogna, E. Riccardi, S. M. A. Sarfraz, G. Scamarcio, and M. S. Vitiello, in *47th International Conference on Infrared, Millimeter and Terahertz Waves (IRMMW-THz)* (IEEE, 2022).
- ³⁷E. O. Polat and C. Kocabas, "Broadband optical modulators based on graphene supercapacitors," *Nano Lett.* **13**, 5851–5857 (2013).
- ³⁸A. C. Ferrari and D. M. Basko, "Raman spectroscopy as a versatile tool for studying the properties of graphene," *Nat. Nanotechnol.* **8**, 235–246 (2013).
- ³⁹D. M. Basko, S. Piscanec, and A. C. Ferrari, "Electron-electron interactions and doping dependence of the two-phonon Raman intensity in graphene," *Phys. Rev. B* **80**, 165413 (2009).
- ⁴⁰J. Yan, Y. Zhang, P. Kim, and A. Pinczuk, "Electric field effect tuning of electron-phonon coupling in graphene," *Phys. Rev. Lett.* **98**, 166802 (2007).
- ⁴¹M. S. Ergoktas, G. Bakan, E. Kovalska, L. W. Fevre, R. P. Fields, P. Steiner, X. Yu, O. Salihoglu, S. Balci, V. I. Falko, K. S. Novoselov, R. A. W. Dryfe, and C. Kocabas, "Multispectral graphene-based electro-optical surfaces with reversible tunability from visible to microwave wavelengths," *Nat. Photonics* **15**, 493–498 (2021).
- ⁴²Y. Malevich, M. S. Ergoktas, G. Bakan, P. Steiner, and C. Kocabas, "Video-speed graphene modulator arrays for terahertz imaging applications," *ACS Photonics* **7**, 2374–2380 (2020).
- ⁴³O. Salihoglu, H. B. Uzlu, O. Yakar, S. Aas, O. Balci, N. Kakenov, S. Balci, S. Olcum, S. Süzer, and C. Kocabas, "Graphene-based adaptive thermal camouflage," *Nano Lett.* **18**, 4541–4548 (2018).
- ⁴⁴S. Rafique, D. Jena, V. Protasenko, R. Yan, M. Zhu, L. Liu, H. G. Xing, and B. Sensale-Rodriguez, "Terahertz imaging employing graphene modulator arrays," *Opt. Express* **21**, 2324–2330 (2013).